80-GT-48

THE AMERICAN SOCIETY OF MECHANICAL ENGINEERS
345 E 47 St., New York, N.Y. 10017

The Influence on the Meridional Impeller Shape on the Energy-Transfer in Centrifugal Compressors

K. Bammert

M. Rautenberg
Professors,
Institute for Turbomachinery,
University of Hannover, Germany

P. Knapp*
Klein, Schanzlin & Becker AG.,
Saarbrücken, Germany

Three radial flow impellers were tested having an elliptic blade shape and identical blade geometry at inlet and exit but different shapes of the meridional contours. The compressor maps with pressure ratios up to 2.9:1 are compared using time-dependent measurements of the static pressure at the shroud and of the flow angles closely downstream of the impeller. From these measurements, the influence of impeller shap on the jet-and-wake flow is discussed. It is shown that with increasing impeller length, the wake zone at the suction side of the blades can be only partially influenced and friction losses become dominant with respect to compressor performance. A smooth curvature of the meridional cross section of the impeller channel leads to a better jet-wake ratio at impeller exit. Accordingly, the performance characteristic shows higher values especially when the mass flow is increased.

NOMENCLATURE

- A = factor of proportionality, kJ/kg K
- a_K = velocity of sound at stagnation conditions upstream of the impeller, m/s
- b = diffuser width, m
- c = absolute velocity, m/s
- d = diameter, m
- h = enthalpy, kJ/kg
- l = length, m
- $M_u = u_2/a_K$ = circumferential Mach number
- $\dot{m}$ = mass flow, kg/s } corrected to 1.01325 bar
- n = rot. speed, rpm } and 288.15 K.
- p = pressure, bar
- PS = pressure side
- R = gas constant, m^2/s^2 K
- r = radius, m
- SS = suction side
- t = time coordinate, s
- T = pitch, m
- u = circumferential velocity, m/s
- $\dot{V}$ = volume flow, m^3/s
- w = relative velocity, m/s
- x = coordinate in flow direction, m
- y = coordinate in circumferential direction, m
- z = axial coordinate, m
- α = flow angle between absolute and circumferential velocity, deg
- β = flow angle between relative and circumferential velocity, deg
- γ = hub angle at inlet, deg
- Δ = difference
- δ = $d_{1,o}/d_2$ inlet diameter ratio
- η = efficiency, %
- $\varkappa$ = isentropic exponent
- λ = d/d_2 = diffuser diameter ratio
- ν = $d_{1,i}/d_2$ hub to tip ratio
- π = pressure ratio
- ϱ = density, kg/m^3
- τ = temperature ratio
- φ = inlet flow coefficient and angular coordinate, deg
- ω = angular velocity, 1/s

Subscripts

- K = stagnation condition upstream of the impeller
- i = hub = inner
- o = shroud = outer
- r = radial

*Formerly Research Assistant at the Institute for Turbomachinery.

Contributed by the Gas Turbine Division of The American Society of Mechanical Engineers for presentation at the Gas Turbine Conference & Products Show, New Orleans, Louisiana, March 10-13, 1980. Manuscript received at ASME Headquarters December 10, 1979.
Copies will be available until December 1, 1980.

s = isentropic

tot = total

u = circumferential

1 = impeller inlet

2 = impeller exit

Superscripts

- = mean value

INTRODUCTION

The experimental and theoretical investigations of the flow in centrifugal compressor impellers are complicated because the flow in the impeller is always accompanied by flow separations. These flow separations jeopardize the energy transfer in the rotor and the energy conversion in the diffuser. Thus the question arises if the shape of the impeller has an impact on the origin and development of the wake flow. However, this objective is subject to the restriction, that flow separation in a centrifugal impeller of considerable loading cannot be prevented. This was pointed out repeatedly by various authors (1, 2, 3)+.

Some theoretical and experimental results obtained from three different impellers are presented and discussed. These rotors have an identical blade geometry at entrance and exit of the wheel. They differ only in the flow path in between. Performance characteristics are combined with flow investigations employing nonsteady measuring techniques to facilitate the comparison between the different impellers.

TEST IMPELLERS

A rotor with radially ending blades and a total pressure ratio $\pi_{tot} \approx 3$ was chosen to study the questions mentioned above. Such rotors are frequently used in turbochargers. The measurements were carried out on a test rig in our institute for turbomachinery at the University of Hannover. Power and speed limitations of this rig determined the impeller tip diameter $d_2 = 180$ mm. The blade geometry at impeller inlet, i.e. blade angle, blade height and inlet diameter ratio $\delta = d_{1,o}/d_2$, was established through an optimization of the flow range. Here $d_{1,o}$ is the outer diameter at impeller inlet. With a given maximum Mach number of the relative velocity at impeller inlet of $M_{w,1,o} = 0.85$ the flow coefficient was found to be

$$\varphi = \frac{\dot{V}_1}{\frac{\pi}{4} \cdot D_2^2 \cdot u_2} = 0.124 \qquad (1)$$

In this equation $\dot{V}_1$ is the volume flow rate

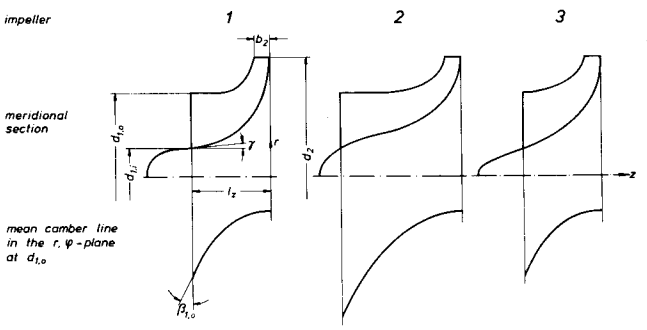

	1	2	3
inlet diameter ratio $\delta = d_{1,o}/d_2 =$	0.7	0.7	0.7
hub to tip ratio $\nu = d_{1,i}/d_2$	0.225	0.225	0.225
exit width ratio $b_2/d_2 =$	0.065	0.065	0.065
length ratio $l_z/d_2 =$	0.325	0.5	0.325
inlet blade angle $\beta_{1,o} =$	27°	27°	27°
hub angle $\gamma =$	4.7°	30°	19°
number of blades	15	15	15

Fig. 1 Test impellers of different meridional flow path

based on upstream stagnation conditions and u_2 is the circumferential tip velocity of the impeller. An elliptical shape of the mean camber line of the blades was selected according to the results reported by Johnson, Ginsburg (4) and Bhinder, Ingham (5). The curvature of the mean camber line extends into the radial part of the rotor, to achieve low loading in the axial part and to avoid a discontinuous transition from the curved to the straight portion of the blade. Hence these impellers differ from the classical "inducer-radial impeller" arrangement. In cross sections normal to the axis of rotation the blades extend in a purely radial direction. Therefore the impellers are made out of aluminium in spite of circumferential tip velocities up to $u_2 = 377$ m/s.

Fig. 1 gives a general view of the chosen impeller shapes. The flow paths in the meridional plane and the mean camber lines in an r, φ-plane are shown, where $r = d_{1,o}/2$. In addition the important geometrical parameters are listed. It is seen that impeller 2 differs from impeller 1 mainly in its larger length ratio. A flow calculation procedure similar to that of Baljé (6) was used to determine the shape of the impeller channel. The idea in selecting the shape of impeller 2 was to reduce the turning and the deceleration per unit path length, in order to lower the tendency of the flow to seperate. It was expected that this reduces the wake extension at impeller exit and thus the mixing losses in the diffuser. This advantage should at least balance the higher friction losses resulting from a longer flow path.

Impeller 3 differs from impeller 1 merely in the hub and shroud line. In impeller 3 the streamlines begin to turn to the radial direction already in the axial part. This results in a higher energy transfer in the inlet region of the impeller using the same blade curvature. Moreover, the axial inflow is turned to the radial discharge with a

+ Numbers in parentheses designate References at end of paper.

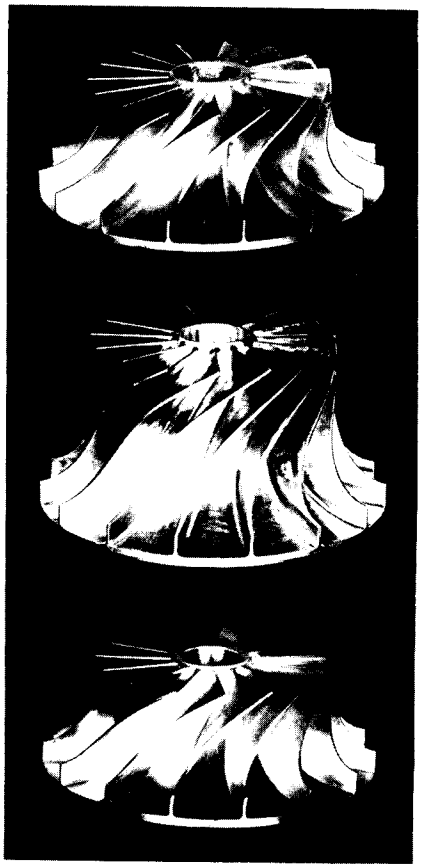

Fig. 2 Test impellers

lower meridional curvature based on the same axial impeller length. This should have a favourable influence upon the flow separation caused by meridional curvature. Fig. 2 shows photographs of the three impellers. They have been manufactured at this institute on a copy milling machine. The material is a wrought aluminium that got the necessary mechanical strength in a cold work-hardening process.

METHODS OF INVESTIGATION

Two approaches were used in the investigation of the different impeller shapes. The flow through the impeller was calculated and detailed measurements were taken. The basis of the calculation is a two-dimensional treatment of the meridional flow by means of a relaxation method as was initially suggested by Wu (7) and supplemented by Schröder (8) with respect to the incidence at the leading edge. Relative velocity, pressure and density resulting from this procedure are used as mean values for a blade-to-blade calculation according to the approximate method by Stanitz (9). Two two-dimensional calculations are combined to a three-dimensional representation of the flow in the impeller. This idealized picture does not account for boundary layers and wake flows. It will be shown later, however, that characteristic phenomena of the real flow can already be seen from the calculations.

The experimental results shall be emphasized in this paper. They are obtained from flow measurements with probes and flush-mounted transducers. For the determination of the performance characteristics probes were used to measure stagnation pressure, stagnation temperature and flow direction at the diffuser exit. The measurements were taken at several positions across the diffuser width. These probes can only give time-average values. To investigate the impeller flow in more detail additional nonsteady transducers were installed to measure the accurate time-dependent values in the highly fluctuating flow that is caused by the rotation of the impeller. Careful static and dynamic calibrations of the measuring systems are essential in this type of measurements, since at the relevant frequencies considerable amplitude and phase distortion is introduced. The fluctuating static pressures were measured along the shroud line of the rotor. For this purpose up to 9 Kulite pressure transducers are mounted flush to the compressor casing. The impeller discharge flow was scanned with a hot wire shadow probe. Such a probe gives the time dependent flow angle α .

RESULTS

The results of the impellers 2 and 3 are compared with those of impeller 1. This impeller 1 is to be understood as the basis of the whole test series.

Fig. 3 shows the comparison of the compressor maps, that were taken with impeller 1 and 2. In the upper part of this figure the total pressure ratio π_{tot} and in the lower part the efficiency η are plotted versus the corrected mass flow $\dot{m}$. Lines of constant efficiency are additionally drawn in the upper diagram. The compressor map gives the stagnation conditions in the diffuser at a diameter ratio $\lambda = d/d_2 = 1.6$ relative to the stagnation condition upstream of the impeller. The efficiency is defined as

$$\eta = \frac{\Delta h_{tot,s}}{\Delta h_{tot}} = \frac{\pi_{tot}^{\frac{\kappa-1}{\kappa}} - 1}{\tau_{tot} - 1} \qquad (2)$$

which is the ratio of isentropic to actual total enthalpy rise. The values for the total enthalpies can be calculated from the measured total pressure and total temperature ratios. Five different speed lines were measured for each compressor map. The range of operation is limited to low mass flow rates by the surge line and to high mass flow rates through a throttle characteristic. This characteristic is the result of a throttle ring that is built into the diffuser to achieve axisymmetric flow within the diffuser and the impeller.

The pressure characteristics of both compressors are rather flat. A clear decrease of the pressure to the surge and the choke line can be seen only at higher speeds. The pressure characteristics are almost identical

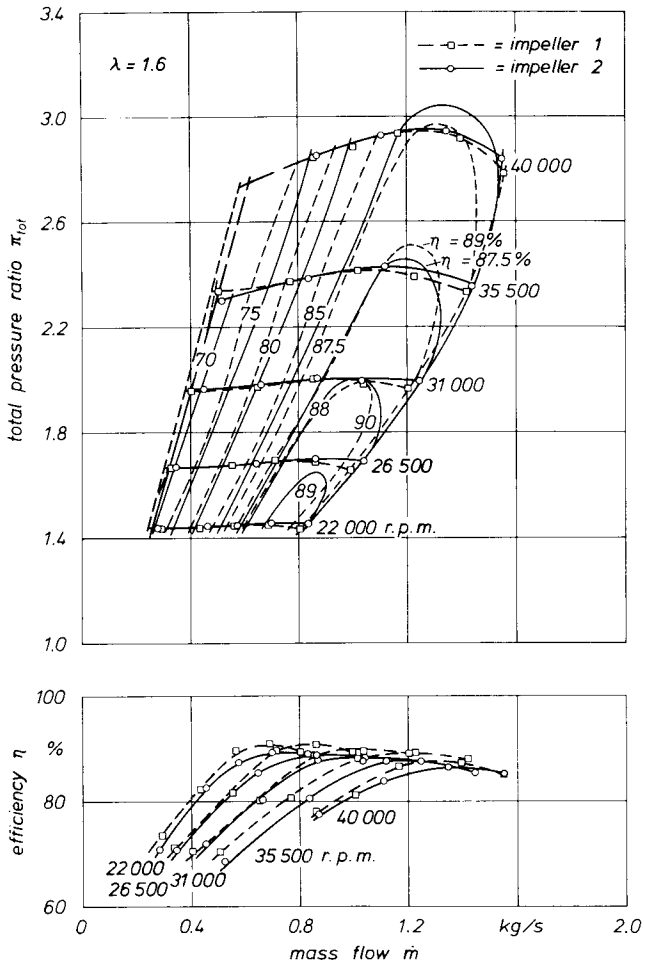

Fig. 3 Comparison of the compressor maps for impeller 1 and 2

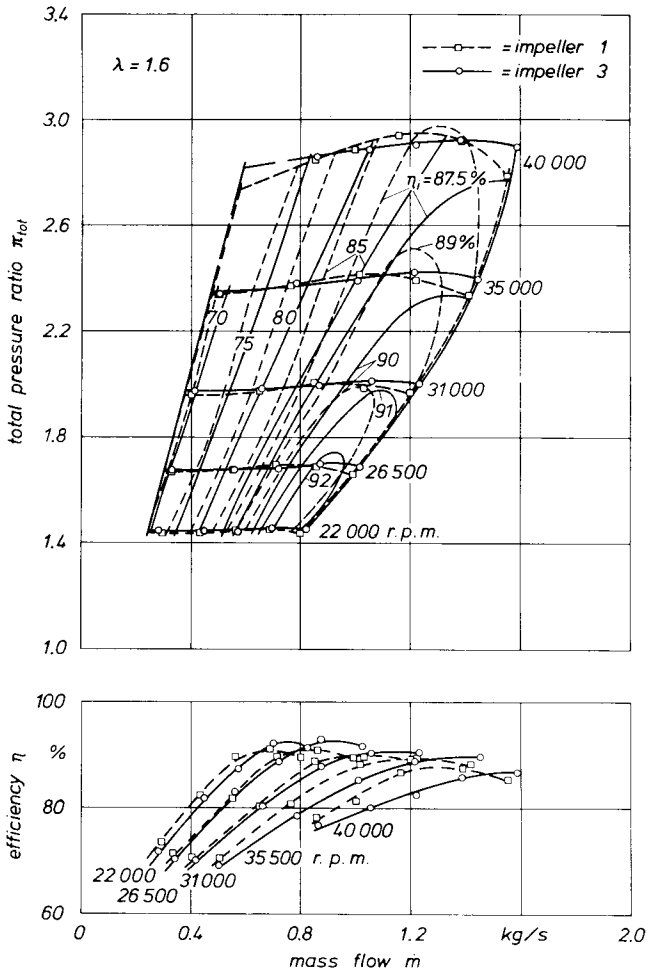

Fig. 4 Comparison of the compressor maps for impeller 1 and 3

in the region of rotating stall, where the efficiency drops significantly. In the efficiency maximum impeller 2 exhibits a slightly higher pressure ratio. However, impeller 2 shows here 1.5 to 2 % points lower efficiency. These results already indicate, that the shape of impeller 2 causes higher losses, reflected in partially lower efficiencies.

Fig. 4 shows the comparison of the compressor maps of impeller 1 and 3. In this case it is even more apparent than with impeller 2, that the maxima of the total pressure lines are shifted towards higher mass flow rates compared with impeller 1. In this range of the map the efficiencies of impeller 3 exceed those of impeller 1. It is noted, that in the case of impeller 3 the efficiency at higher speeds does not decrease towards the choke line. The nominal flow coefficient corresponds to a mass flow rate $\dot{m}$ = 1.46 kg/s at the highest speed. At this operating condition the characteristics of impeller 1 decrease noticeably and lie below those of impeller 3. Regarding the compressor maps it was found, that the differences between the tested impellers are less obvious than expected.

The detailed investigations of the impeller flow were carried out in two operation points on the mean speed line with 31,000 r.p.m. The first point represents the maximum efficiency of impeller 1 and the second lies at maximum flow rate, where the impellers have quite different characteristics. Fig. 5 shows results of the nonsteady measurements of impeller 1 taken at the point of maximum efficiency. Lines of constant static pressure along the shroud line of the impeller are plotted in the lower part of this figure. The values on the curves give the pressure ratio relative to inlet stagnation conditions. These isobars result from pressure signals measured at 8 locations along the inner contour of the compressor casing. In Fig. 5 x designates the distance of the transducer location from the impeller leading edge measured along the shroud line of the blade, and l is the total length until impeller exit. Fig. 5 shows, that there is only a small increase of static pressure up to $x/l \approx 0.5$. Further downstream the pressure gradient in flow direction rises as indicated by the smaller spacing of the isobars. The interpretation of this figure with respect to

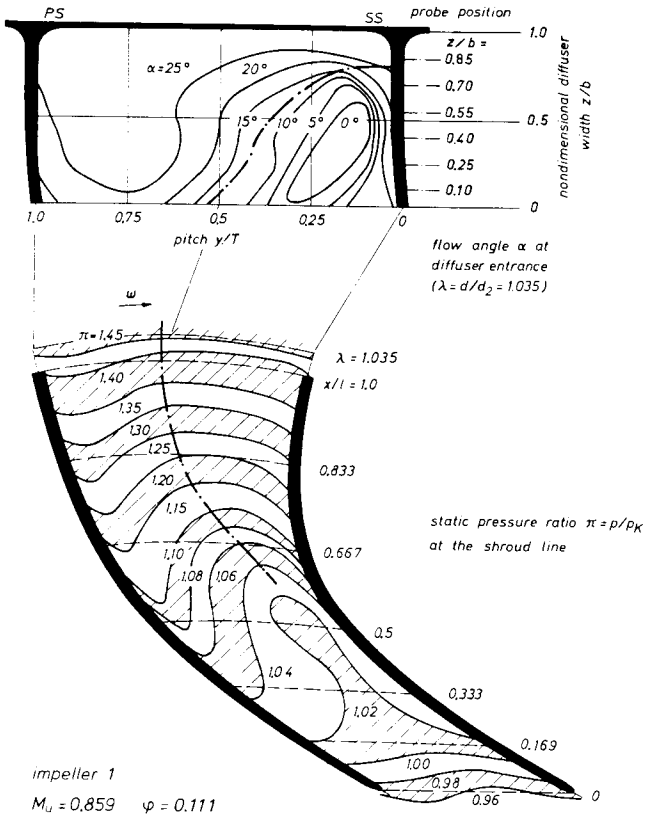

Fig. 5 Pressure and flow angle distribution of impeller 1

flow separation necessitates the use of the nonsteady energy equation. It can be written for adiabatic flow

$$\frac{d h_{tot}}{d t} = \frac{1}{\rho} \cdot \frac{\partial p}{\partial t} \qquad (3)$$

From this equation it becomes obvious, that an energy transfer can only be accomplished with a positive gradient of the static pressure with respect to time. Such a positive gradient is indicated in the isobaric field, when the isobars are perpendicular or inclined against the circumferential direction. Additionally the pressure has to rise towards the pressure side, i.e. from right to left in Fig. 5. No energy is transfered to the fluid, when the isobar is parallel to the circumferential direction and thus the gradient $\delta p / \delta t = 0$. Based on this idea the boundary of the wake flow is defined as the line where the isobars start to differ from the circumferential direction and show a positive pressure gradient. This wake flow boundary is drawn as a dash-and-dot line in the isobaric field. Using this definition the line should have been extended until impeller inlet. But since the pressure fluctuations in this region are small, the influences of wake flow and tip clearance flow cannot be clearly separated. But downstream from a line $x/l > 0.6$ the wake flow grows significantly and reaches its largest extension at $x/l \approx 0.8$. From here on till impeller exit the wake flow occupies more than 50 % of the pitch. Thus energy is transfered to the fluid only in that half of the channel adjacent to the pressure side. This is true at least within the vicinity of the shroud line.

The extension of the wake flow across channel depth will be discussed using the upper part of Fig. 5. In this diagram the flow angle distribution shortly behind impeller exit is plotted in form of lines of constant angle α. The vertical axis gives the width of the diffuser and the horizontal axis the pitch, that is derived from the impeller blade number and the diameter ratio in the diffuser $\lambda = 1.035$. Since α is the angle between the absolute velocity and the circumferential direction a low value of α corresponds to a low radial velocity component and therefore low mass flow. So the angle distribution reveals the wake flow in the corner between diffuser front wall and blade suction side. Taking the wake flow boundary from the pressure distribution along the shroud line a corresponding angle of $\alpha \approx 13^{\circ}$ is found in the angle distribution at the width position $z/b = 0$. Therefore a line following $\alpha = 13^{\circ}$ was defined as wake flow boundary in the upper diagram and is added as a dash-and-dot line. The extension of the wake diminishes rapidly across diffuser width and impeller channel depth, respectively. But the fairly constant spacing of the lines of constant angle indicates that the transition from wake to jet flow ($\alpha > 25^{\circ}$) is quite gradual. This is most probably a result of the mixing process in the diffuser entrance. The transition from jet to wake in the adjacent channel however is much steeper as is obvious from the narrowly spaced lines near the suction side of the blades. In general it can be seen, that the unfavourable picture of the flow at the shroud line is improved within the flow channel.

This fact is illustrated in a different way in Fig. 6. There the factor $\Delta p/\bar{p}$, obtained from theory and measurement, is plotted versus the length of the streamlines in the impeller. Δp represents the pressure difference between pressure and suction side or in case of the measurements the difference between maximum and minimum value. It is devided by the mean value of the static pressure $\bar{p}$. In the undisturbed flow the pressure rises linearly with respect to time and so $\Delta p/\bar{p}$ can be related to the energy equation in the following way

$$\frac{d h_{tot}}{d t} = \frac{1}{\rho} \cdot \frac{\partial p}{\partial t} \approx \frac{R \cdot T}{\bar{p}} \cdot \frac{\Delta p}{\Delta t} = A \cdot \frac{\Delta p}{\bar{p}} \qquad (4)$$

In this equation A is a factor of proportionality that does not vary significantly along the flow path if compared with $\Delta p/\bar{p}$. Hence the latter is a measure for the energy transfered and can also be understood as a factor

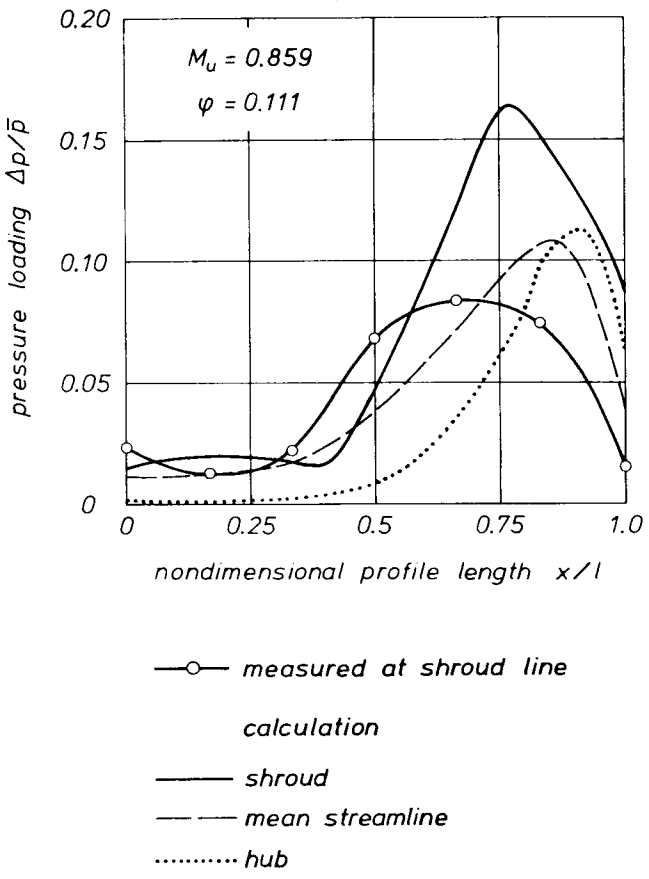

Fig. 6 Blade loading of impeller 1

of loading. Fig. 6 shows graphs of $\Delta p/\bar{p}$, that are obtained from the three-dimensional, calculated flow distribution. First the one at the shroud line shall be discussed. In the inlet region of the impeller the blade loading is low and the energy transfered to the fluid is small. At x/1 = 0.4 the shroud line starts to curve outward and as a result the flow is accelerated. This leads to a slight decrease of the loading. Thereafter the loading rises steeply until x/1 ≈ 0.8 and decreases again till impeller exit. The circles give the corresponding values of the measurements. They also show low loading in the inlet region. Because of the boundary layers, that are not incorporated in the calculation, the acceleration due to the curvature of the shroud line is reduced. Thus the increase of loading in the real flow starts earlier and maintains a steep gradient up to x/1 ≈ 0.5. The maximum, reached at x/1 = 0.67, is significantly lower than the theoretically predicted value. Then the loading decreases progressively towards the exit. A comparison of Fig. 6 with Fig. 5 suggests that the wake flow begins to occupy a considerable portion of the flow channel at about the same x/1, where the measured loading begins to deviate from the calculated curve. This deviation increases along with an increase in wake flow extension up to x/1 ≈ 0.8. From there on the curves in Fig. 6 are almost parallel and the wake flow extension remains constant. Inside the impeller channel, where only the calculated loading values are available, the maximum blade loading decreases remarkably. The dashed line illustrates the development along the mean streamline and the dotted line along the hub. The flow is likely to sustain a low pressure loading more easily and accordingly the flow angle distribution in Fig. 5 shows a considerable decrease of wake flow extension.

Therefore, two effects seem to be favourable for the limitation of the wake development, although the wake cannot be entirely prevented. 1) The theoretical blade loading, i.e. the energy transfer, should reach its maximum value fairly early along the flow path and decrease gradually to the end of the impeller. It will be shown later, that this depends on impeller geometry. 2) A steep reduction in loading with channel depth.

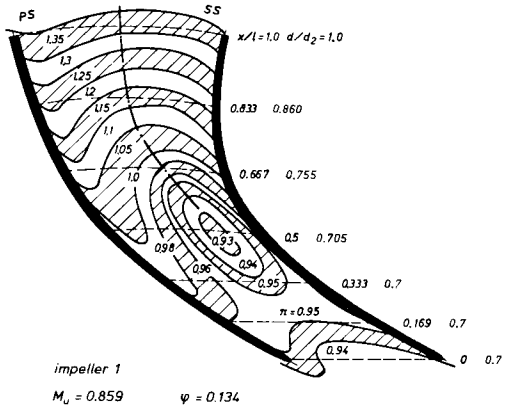

Fig. 7 Static pressure along shroud line of impeller 1

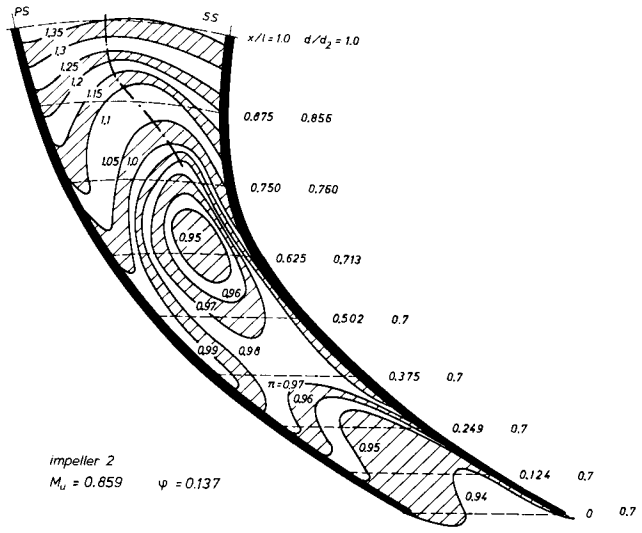

Fig. 8 Static pressure along shroud line of impeller 2

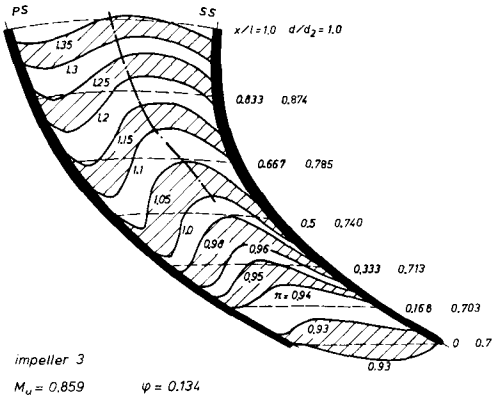

Fig. 9 Static pressure along shroud line of impeller 3

In Fig. 7 the pressure distribution is plotted for impeller 1 at the higher mass flow rate. This figure shall be compared with Fig. 8 and Fig. 9, where the corresponding distributions are for the impellers 2 and 3. Impeller 1 shows a characteristic pressure minimum half way through the impeller, that was not as pronounced at the lower mass flow rate. In the radial part of this impeller, $x/l \geq 0.5$, the pressure starts to rise. Similar conditions are found for impeller 2 in Fig. 8. In this case the pressure minimum is located at a larger x/l. Similar to impeller 1 this location of the pressure minimum corresponds to the beginning of shroud line curvature, that causes flow acceleration. Concerning flow separation impeller 2 experiences a strong increase in wake extension between $x/l \approx 0.75$ and 0.9. Compared with impeller 1 the flow in impeller 2 begins to separate not only at a larger x/l but also at a larger diameter ratio d/d_2. Thus the more gradual turning of the flow seems to have positive influence. However, at impeller exit both impellers have the same wake flow extension and the advantage of impeller 2 has disappeared.

The modified meridional shape of impeller 3 produces a more uniform pressure rise in flow direction than in impeller 1. The isobars in Fig. 9 show this clearly. They have a similar character throughout the whole impeller. Contrary to impeller 1 no pressure minimum is found in this impeller. Such a uniform pressure rise was expected to reduce the tendency of the flow to separate. The wake boundary drawn in Fig. 9 shows, however, that in comparison with impeller 1 the wake extension across the pitch is almost the same in both wheels. The mere difference is, that in impeller 3 the maximum wake extension is reached at impeller exit, whereas in impeller 1 it is found already at $x/l \approx 0.8$.

The wake flow behavior of the three impellers shall additionally be discussed using the pressure loading diagrams, that are shown in Fig. 10. In impeller 2 and 3 the maximum predicted loading along the shroud line is reached shortly before impeller exit. This is in clear opposition to impeller 1. Comparing with the measured values it is seen,

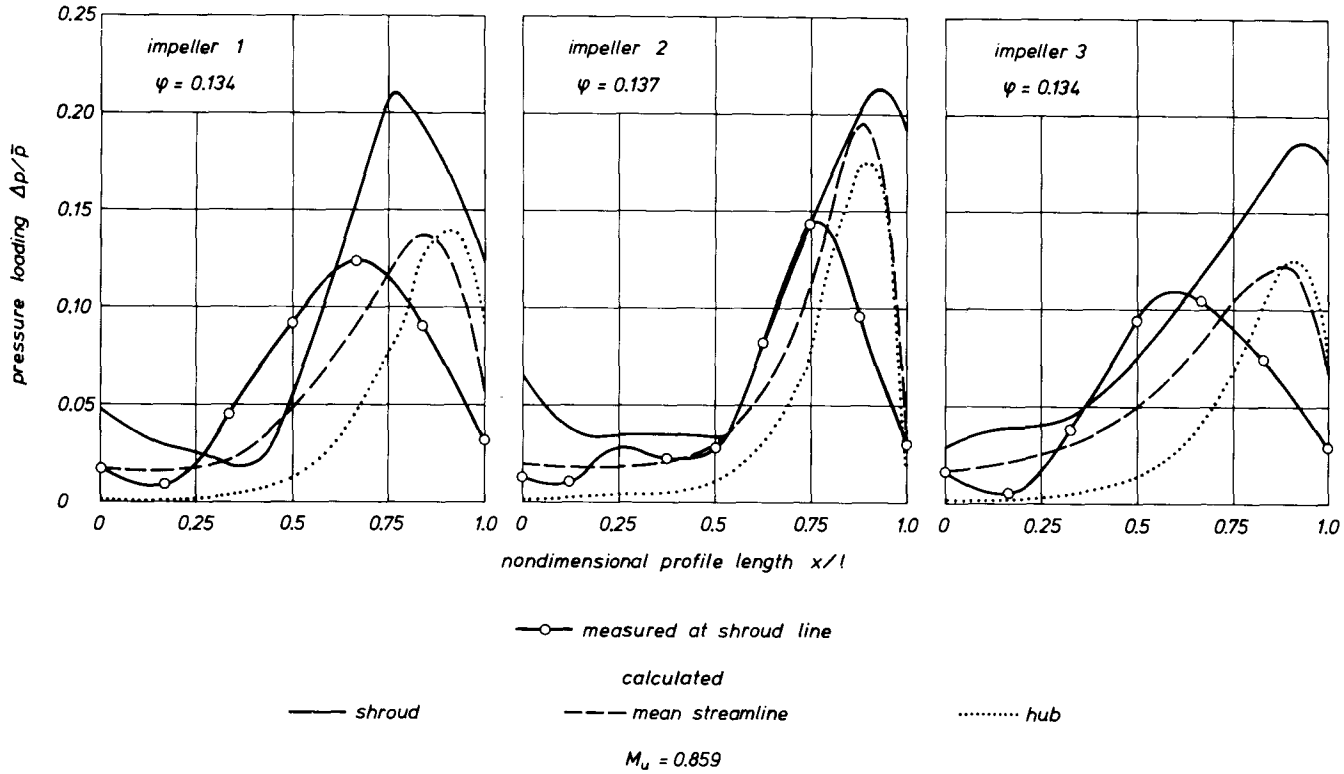

Fig. 10 Blade loading of impeller 1, 2 and 3

that the flow in impeller 2 can follow the predicted curve fairly well up to x/l = 0.75. Further downstream there is a considerable difference between calculation and measurement. Owing to flow separation at the suction side the measured loading decreases strongly towards impeller exit. The maximum local energy transfer at x/l = 0.75 is higher than in the other two impellers. Comparing Fig. 8 and Fig. 10 it is found to be true also for this impeller, that the difference between measurement and calculation increases, where the wake extension grows. Downstream x/l $\approx$ 0.9 the curves of the loading are almost parallel and the wake extension remains constant. The same qualitative agreement of the difference between calculated and measured pressure loading and wake extension is found in impeller 3. Moreover, in this rotor the loading begins to rise right at the impeller inlet. Since the flow approaches the blades with incidence, the higher energy transfer in impeller 3 cannot be detected in the real flow. The measured curves of impeller 1 and 3 hardly differ in the inlet region.

The calculated pressure loading along the mean streamline and also the hub show finally, that impeller 2 achieves also very high loading values within the flow channel. In this respect the loading conditons within the other two impellers are definitely better. Thus it can be noted for impeller 2, that a slight indication of a reduced tendency to separate is achieved. But owing to mixing losses of the same magnitude as with impeller 1 and higher friction losses the overall efficiency is lower.

The comparison of impeller 1 and 3 shall be concluded using the flow angle distributions in Fig. 11. At the lower mass flow rate both impellers have the same characteristic parameters. Except at the front wall it is apparent, that behind impeller 3 the region of low flow angles ($\alpha < 0^{o}$) extends less in circumferential direction than behind impeller 1.

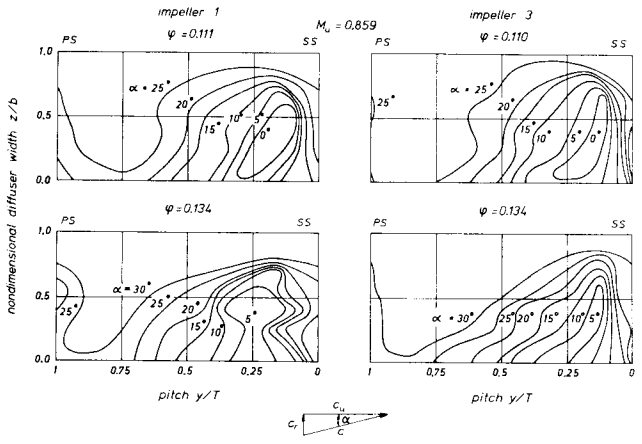

Fig. 11 Flow angle distribution downstream of impeller 1 and 3

Besides that no significant difference exists between the two impellers. This changes when the mass flow is increased. At φ = 0.134 the region of low flow angles behind impeller 3 is reduced and occupies, in form of a triangle, the corner between the diffuser front wall and the suction side of the blade. The wake width, that is approximately given by the 15^{o}-isocline, decreases steadily across the diffuser. Thus the conditions within the flow channel are much better than at the shroud. Behind impeller 3 the variation of the flow angle in circumferential and axial direction is very gradual, as is indicated by the constant distance of the isoclinic lines. Behind impeller 1 the 5^{o}-isocline circumscribes a comparatively large region in the middle of the channel. The closely spaced isoclines refer to steeper gradients than behind impeller 3. The 15^{o}-isocline, taken as the wake flow boundary, forms a somehow trapezoidal region, so that here the wake flow decreases less rapidly across diffuser width. From this it is concluded, that the mixing of jet and wake behind impeller 3 at this mass flow generates lower losses and results in higher pressure and efficiency values in the compressor map.

SUMMARY

Three impellers of different meridional flow paths have been investigated experimentally and theoretically. It was the objective to reduce the extent of flow separation by means of impeller shaping, although it was realized, that separation could not be avoided altogether. The chosen impeller shapes could only partially accomplish this aim. However, the comparison between calculation and measurement showed, that an effort should be made in the design process to achieve a reduction of blade loading towards the impeller exit. This can be accomplished for instance with backswept blades.

ACKNOWLEDGEMENT

The investigations dealt with in this paper have been carried out within the framework of the Special Research Programme (SFB 61) of the German Research Association (DFG). The authors thank them for their support.

REFERENCES

1 Dean, R.C., "On the Unresolved Fluid Dynamics of the Centrifugal Compressor", Advanced Centrifugal Compressors, ASME 1971.

2 Bammert, K., M. Rautenberg, "Die Energieübertragung in hochbelasteten Radialverdichtern", Conf. for Compressors "SYMKOM 77", Lodz, Poland, Nov. 1977.

3 Traupel, W., "Grundzüge einer Theorie des radialen Verdichterlaufrades", Forschungsberichte Verbrennungskraftmaschinen, Heft 157, 1974.

4 Johnson, I.A., A.Ginsburg, "Some NACA-Research on Centrifugal Compressors", Trans. ASME, July 1953.

5 Bhinder, F.S., D.R. Ingham, "The Effect of Inducer Shape on the Performance of High Pressure Ratio Centrifugal Compressors", ASME-Paper No. 74-GT-122, 1974.

6 Baljé, O.E., "Loss and Flow Path Studies on Centrifugal Compressors-Part I/II", ASME-Paper No. 70-GT-12-a/b, 1970.

7 Wu, Ch. H., "A General Theory of Three-Dimensional Flow in Subsonic and Supersonic Turbomachines of Axial, Radial and Mixed Flow Types", NACA-TN 2604, 1952.

8 Schröder, H.J., P. Schuster, "Actuator Disc Flow Calculated by Relaxation - An Approach to the Analysis Problem of Turbomachinery", ASME-Paper No. 72-GT-26, 1972.

9 Stanitz, J.D., V.D. Prian, "A Rapid Approximate Method for Determining Velocity Distribution on Impeller Blades of Centrifugal Compressors", NACA-TN 2421, 1951.